Ab initio study of the structural and optical properties of orthorhombic ternary nitride crystals

Jung Y Huang[1,3]**, L-C Tang**[1] **and M H Lee**[2]

[1] Institute of Electro-Optical Engineering, Chiao Tung University, Hsinchu 305, Taiwan, Republic of China
[2] Department of Physics, Tamkang University, Taipei 251, Taiwan, Republic of China

E-mail: jyhuang@cc.nctu.edu.tw

Abstract
The structural, optical and mechanical properties of orthorhombic ternary nitride crystals have been analysed theoretically with first-principles calculation. Our results indicate that these nitrides possess fairly large optical bandgap (4–6 eV), second-order nonlinear optical susceptibility (13–18 pm V^{-1}), and bulk modulus 170–370 GPa. Therefore these materials could be useful for optical and protective coating applications. Our analysis with the band-by-band and atomic species projection techniques not only yields useful information about material properties, but also provides deep insight into the fundamental understanding of the mechanical and optical properties of orthorhombic ternary nitrides.

(Some figures in this article are in colour only in the electronic version)

1. Introduction

Nitrogen, like carbon, has an inclination to form multiple bonds, which distinguishes it from the other group VB elements. The properties of the numerous covalent nitrides vary greatly depending on the element with which nitrogen is combined. For example, the optical bandgap of compound semiconductors formed from group III elements and nitrogen varies from 6.5 eV for AlN to 2 eV for InN. Therefore group III–N alloys can be used to fabricate optical active devices with output wavelengths covering from the red to the ultraviolet [1]. Nitrides of a number of metals can also form hard and highly stable refractory materials with very high melting points. These materials recently have attracted significant interest for their potentials as protective or wear resistant coating layers.

The chemistry of nitrogen in many aspects of the structure of alloys is still not well understood [2]. Orthorhombic ternary nitrides are relatively new ceramic materials with
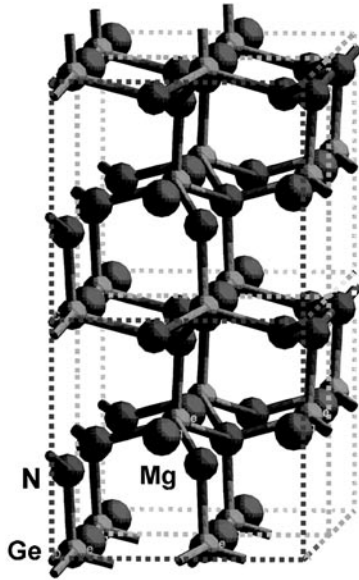
[3] Addressee for correspondence.

Figure 1. The crystal structure of orthorhombic ternary nitride MgGeN$_2$ with $Pna2_1$ symmetry.

potentially interesting thermal, mechanical and optical properties [3]. These crystals are therefore of technological and scientific importance. However to fully realize their potential, sufficient understanding in these ternary nitrides is essential. Electronic structure calculations can provide much insight into materials with existing and possibly new structures.

In this paper, theoretical studies on the electronic structures, mechanical and optical properties of orthorhombic ternary nitrides with first-principles calculation are presented. We do not intend to produce most accurate values for comparing with experimental results since no such data are currently available. Instead we aim at improving the fundamental understanding of the mechanical and optical properties of orthorhombic ternary nitrides.

2. Method

The crystal structure of an orthorhombic ternary nitride ABN$_2$ is shown in figure 1. The unit cell has $Pna2_1$ symmetry [3]. The metal atoms A, B and the two crystallographically different N atoms occupy the general positions (x, y, z; $\bar{x}$, $\bar{y}$, $z + 1/2$; $x + 1/2$, $\bar{y} + 1/2$, z; $\bar{x} + 1/2$, $y + 1/2$, $z + 1/2$). Both metal atoms are tetrahedrally coordinated by N and vice versa both N atoms are tetrahedrally coordinated by the two metal atoms. This crystal structure with lattice constants a, b and c can also be deduced from a hexagonal structure ($a' = b'$, c') in which $a \approx \sqrt{3}a'$, $b \approx 2a'$ and $c = c' \approx \sqrt{8/3}a'$.

The calculations were performed using the *ab initio* plane-wave-pseudopotential approach within the framework of density-functional theory (DFT) implemented in CASTEP software [4]. The summation over the Brillouin zone (BZ) was carried out with a k-point sampling using a Monkhorst–Pack grid [5]. A kinetic-energy cutoff of 550 eV and 18 k special points and 96 bands were used to ensure the convergence in the calculations of optical properties. In order to save computation time, the size of the special point set was reduced to eight k points ($3 \times 3 \times 3$ mesh) for the calculations of the equilibrium lattice constants and mechanical properties. We found that the smaller set of k points causes less than 2% difference in the equilibrium lattice constants.

2.1. Calculations of structural properties

The equilibrium lattice constants and fractional atomic coordinates are determined from the total-energy minimization procedure. We carried out the relaxation of the lattice parameters and atomic positions within constraints imposed by the space-group symmetry elements. Energy–volume relations were obtained by varying unit-cell volumes and the results were fitted to the Murnaghan equation of state [6]

$$E_{\text{tot}}(V) = \frac{B_0 V}{B_0'} \left[\left(\frac{V_0}{V} \right)^{B_0'} \frac{1}{B_0' - 1} + 1 \right] + E_0. \tag{1}$$

From the fit, an estimate of the static bulk modulus at zero pressure B_0, and the first-order pressure derivative of the bulk modulus B_0' can be obtained. This procedure has proved to be quite reliable in the computational design of advanced materials.

In this work, we derive the phonon frequencies of ABN_2 with the Hellmann–Feynman (HF) forces and the direct method [7]. The calculations start from building a $1 \times 1 \times 1$ supercell with an optimized geometry. For this configuration, the maximal magnitude of the HF forces does not exceed 0.001 eV Å^{-1}. The HF forces are then calculated for displaced atoms, one at a time. We have displaced atoms A, B, N(1) and N(2) along x, y, and z directions by an amplitude of 0.03 Å. Each displaced configuration generated $3 \times 16 = 48$ components of HF forces and a total of 576 components have been used to construct the dynamical matrix and deduce the phonon frequencies [8].

2.2. Calculations of electronic properties

To understand the nature of optical transitions and other relevant effects on the calculated optical properties, we study the local densities of states and other electronic properties of these nitride crystals.

Let $\Psi_{nk}(\vec{r})$ be the self-consistent wave function of the crystal at the nth band and kth point in the BZ; we can decompose $\Psi_{nk}(\vec{r})$ into a summation over the atomic orbitals $\{\Phi_{lm}^{(i)}(\vec{r})\}$ of each atomic species i by

$$\Psi_{nk}(\vec{r}) = \sum_{i \in \{\text{atoms}\}} \sum_{l} \sum_{m=-l}^{m=+l} C_{nk,lm}^{(i)} \Phi_{lm}^{(i)}(\vec{r}) \tag{2}$$

where $C_{nk,lm}^{(i)} = \int_{V_0} \Psi_{nk}(\vec{r}) \Phi_{lm}^{(i)*}(\vec{r}) \, dV$. The lth orbital of the α species contributes to $\Psi_{nk}(\vec{r})$ by a fraction of $h_{nk,l}^{(\alpha)}$ [9]

$$h_{nk,l}^{(\alpha)} = \left(\sum_{i \in \{\alpha\}} \sum_{m=-l}^{m=+l} C_{nk,lm}^{(i)} C_{nk,lm}^{(i)*} \right) \left(\sum_{i \in \{\alpha, \beta, \gamma, \ldots\}} \sum_{l} \sum_{m=-l}^{m=+l} C_{nk,lm}^{(i)} C_{nk,lm}^{(i)*} \right)^{-1}. \tag{3}$$

An atom projection concept was then employed for resolving interesting components from the total density of states (TDOS)

$$\text{LDOS}(\alpha, E) = \sum_{n} \sum_{k} \sum_{l} h_{nk,l}^{(\alpha)} \delta(E - E_{nk})$$

$$\text{PDOS}(\alpha l, E) = \sum_{n} \sum_{k} h_{nk,l}^{(\alpha)} \delta(E - E_{nk}). \tag{4}$$

The partial density states (PDOS) and local density of states (LDOS) can be used to provide valuable insight into the formation of the energy bandgap and the nature of transitions from which the linear and nonlinear optical properties originate.

2.3. Calculations of linear and nonlinear optical properties

In a crystalline solid, the most important optical transitions do not change the momentum or the spin of the electrons involved in the transition. In terms of an energy band structure this means that one has to consider optical excitations from an occupied to unoccupied state of the same spin for each k vector in the BZ.

The linear optical properties of a dielectric crystalline material can therefore be described with a dielectric function of $\varepsilon_{ij}(\vec{q}, \omega)$ at $\vec{q} = 0$. When the incident photon energy is higher than the bandgap E_g, the material can attenuate the photon flux. The absorption coefficient $\alpha_{ij}(\omega)$ is related to the imaginary part of the dielectric function by [10]

$$\operatorname{Im} \varepsilon_{ij}(\omega) = \frac{\lambda n(\omega)}{2\pi} \alpha_{ij}(\omega) = \frac{8\pi^2 \hbar^2 e^2}{m^2 V} \sum_k \sum_{cv} (f_c - f_v) \frac{p_{cv}^i(k) p_{vc}^j(k)}{E_{vc}^2} \delta[E_{cv}(k) - \hbar\omega]$$

$$= \frac{5.2324 \times 10^3}{V(\text{Å}^3)} \sum_k \sum_{cv} \frac{p_{cv}^i(k, \text{Å}^{-1}) p_{vc}^j(k, \text{Å}^{-1})}{E_{vc}^2} \delta[E_{cv}(k, \text{ eV}) - \hbar\omega]. \quad (5)$$

Here f_c represents the Fermi distribution of the conduction band c; $p_{cv}^i(\vec{k}, \text{Å}^{-1})$ denotes the momentum matrix element (MME, in unit of Å^{-1}) from the conduction band c to the valence band v at the k point of the BZ. The real part of the dielectric function was obtained from the imaginary part with Kramer–Kronig transformation.

For the second-order nonlinear optical response, the theoretical description is much more complex [11]. However, it is fairly easy to derive the NLO susceptibility at the zero frequency limits

$$\chi_{ijk}^{(2)}(0) = \frac{1}{V} \left(\frac{e\hbar}{m}\right)^3 \sum_k \sum_{vc} \left[\sum_{c'} \frac{1}{E_{c'c} E_{cv}^2 E_{c'v}^2} (D_{vc'c}^{ijk} + D_{cvc'}^{ijk} + D_{c'cv}^{ijk}) \right.$$

$$\left. - \sum_{v'} \frac{1}{E_{vv'} E_{cv}^2 E_{c'v}^2} (D_{v'cv}^{ijk} + D_{vv'c}^{ijk} + D_{cvv'}^{ijk}) \right] \quad (6)$$

where $D_{nml}^{ijk} = \operatorname{Im}[p_{nm}^i(p_{ml}^j p_{\ln}^k + p_{ml}^k p_{\ln}^j]/2$. We are interested in decomposing $\chi_{ijk}^{(2)}(0)$ into various contributions from atomic species or orbitals. This can be properly done by calculating the contribution from the αth species as [12]

$$\chi_{ijk}^{(2)}(\alpha, E) = \frac{1}{V} \left(\frac{e\hbar}{m}\right)^3 \sum_l \sum_k \sum_{vc} [h_{vk,l}^{(\alpha)} \delta(E - E_{vk}) + h_{ck,l}^{(\alpha)} \delta(E - E_{ck})]$$

$$\times \left[\sum_{c'} \frac{(D_{vc'c}^{ijk} + D_{cvc'}^{ijk} + D_{c'cv}^{ijk})}{E_{c'c} E_{cv}^2 E_{c'v}^2} - \sum_{v'} \frac{(D_{v'cv}^{ijk} + D_{vv'c}^{ijk} + D_{cvv'}^{ijk})}{E_{vv'} E_{c'v}^2 E_{cv}^2} \right]. \quad (7)$$

Equation (7) is very similar to equation (4) except that the second-order nonlinear optical strengths serve as the weighting factor. We shall use this equation to yield insight into the underlying mechanism of NLO susceptibility.

3. Results

3.1. Crystal structure and lattice dynamical properties

The calculated atomic positions of six orthorhombic ternary nitride crystals are summarized in table 1. The tetrahedral coordination of the N atoms is distorted with the presence of two

Table 1. Calculated fractional atomic coordinates of the orthorhombic ternary nitrides.

Nitride crystal ABN$_2$ ($Pna2_1$)	Fractional coordinates of metal A	Fractional coordinates of metal B	Fractional coordinates of species N
BeCN$_2$	Be (0.088, 0.677, 0.000)	C (0.057, 0.130, −0.007)	N1 (0.058, 0.100, 0.345)
			N 2(0.124, 0.659, 0.390)
MgCN$_2$	Mg (0.088, 0.677, 0.000)	C (0.046, 0.125, 0.002)	N 1 (0.035, 0.061, 0.330)
			N2 (0.117, 0.670, 0.444)
BeSiN$_2$	Be (0.086, 0.656, 0.003)	Si (0.078, 0.129, −0.007)	N1 (0.083, 0.126, 0.372)
			N2 (0.096, 0.633, 0.360)
MgSiN$_2$	Mg (0.076, 0.625, 0.000)	Si (0.068, 0.125, 0.010)	N1 (0.051, 0.093, 0.355)
			N2 (0.112, 0.657, 0.421)
BeGeN$_2$	Be (0.115, 0.660, 0.000)	Ge (0.082, 0.129, −0.012)	N1 (0.070, 0.126, 0.368)
			N2 (0.091, 0.635, 0.358)
MgGeN$_2$	Mg (0.076, 0.625, 0.000)	Ge (0.069, 0.125, 0.010)	N1 (0.053, 0.096, 0.357)
			N2 (0.110, 0.654, 0.418)

types of metal–N bond. The average bond length is calculated to be 1.75 Å for Si–N and 2.09 Å for Mg–N. These results agree well with the recent measured values of MgSiN$_2$ with the neutron diffraction method [13]. The contours of charge difference in the MgSiN$_2$ crystal on a plane perpendicular to the z axis are shown in figure 2. The electron density is much lower around the group IV atom (Si) relative to the N, indicating strong directionality of Si–N bonding. Comparing to the group-IV homo-nucleus semiconductors, the stronger bonding between group IV and N atoms leads to a shorter bond length and therefore a larger energy bandgap. This tendency can be better appreciated in figure 3, where comparisons of the optical bandgap of orthorhombic ternary nitride crystals, column IV and IV nitrides as a function of bond length are shown.

In figure 4, we present the calculated energies as a function of unit cell volume for the two orthorhombic ternary nitride crystals BeCN$_2$ and MgCN$_2$. From the calculated results, the equation-of-state parameters such as the bulk modulus and its pressure derivative were deduced. The results are summarized in table 2. The bulk modulus for MgCN$_2$ was found to be 234 GPa, which decreases to 175 GPa for MgSiN$_2$ and 171 GPa for MgGeN$_2$. The tendency is expected from the decreasing bonding strength (and therefore larger unit cell volume) from C–N, Si–N to Ge–N. By replacing Mg with Be, the bulk modulus becomes even larger with a value reaching 374 GPa for BeCN$_2$. These calculated values support the notion of the orthorhombic ternary nitrides as potential protective coating materials. Note that our calculated bulk modulus of MgSiN$_2$ also agrees with the linear thermal compressibility $K = 6.84 \times 10^{-12}$ Pa^{-1} ($K \equiv -1/V(\partial V/\partial P)_T = 1/B$) reported in the literature [13]. For further comparison, note that Karch et al estimated the bulk modulus of β-Ge$_3$N$_4$ to be about 214 GPa [15] and Gavrilenko reported 2H-GaN to be 215 GPa [16]. Both crystals possess a similar structure as the ternary nitrides studied here.

The phonons of the orthorhombic ternary nitrides at the Γ point can be classified by the irreducible representation of the point group C$_{2v}$. The group theory predicts the following symmetry of the modes: 12A$_1$ + 12A$_2$ + 12B$_1$ + 12B$_2$, where A$_1$, B$_1$ and B$_2$ modes are both Raman and infrared active while A$_2$ are infrared active only.

There exists a gap from 20 to 250 cm^{-1} in the zone-centre phonon frequencies. We are interested in the high frequency phonon modes since these vibration modes could potentially influence the infrared absorption edge of the ternary nitride crystals. Calculated frequencies
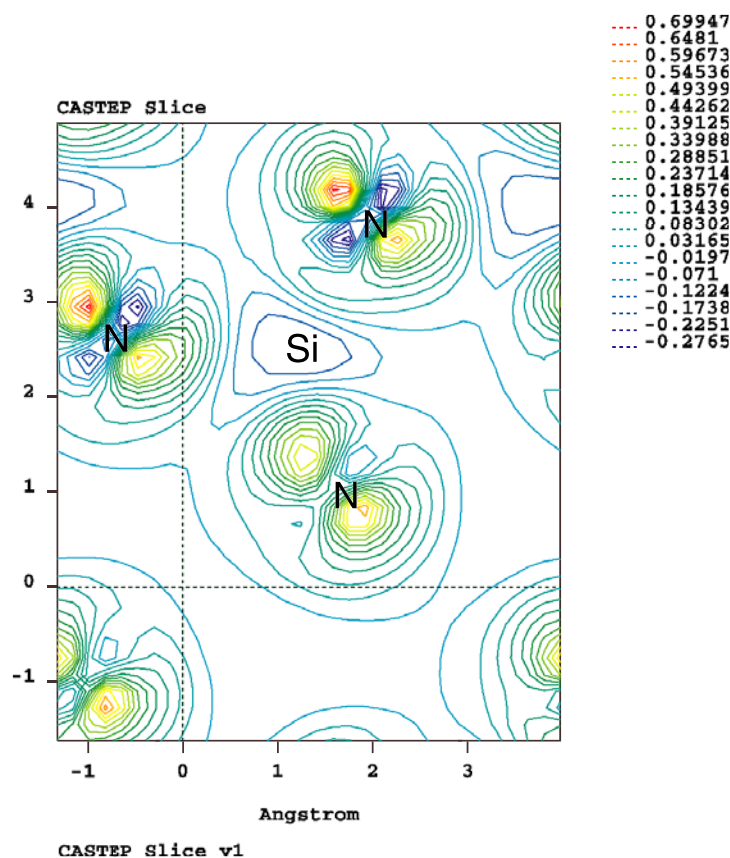
Figure 2. Charge difference contours on a plane perpendicular to the *z* axis of MgSiN$_2$ at a height of 2.05 Å.

of the high-frequency zone-centre photon modes of MgSiN$_2$ and MgGeN$_2$ are summarized in table 3. By replacing Si with Ge, a large frequency downshift appears in the phonon modes whose lattice distortion involves a significant Si motion. These vibrations include the B$_1$-symmetry modes at 465 cm^{-1} and 549 cm^{-1} and A$_1$-symmetry modes at 346, 354, 614, 824 and 836 cm^{-1}. The highest frequency mode at 836 cm^{-1} is Raman and infrared active and therefore could play the major role in determining the infrared absorption edge of MgSiN$_2$. By allowing the possibility of biphonon absorption, MgSiN$_2$ could therefore be transparent up to 6 μm in the infrared.

3.2. Electronic structures and density of states

The electronic band structures of BeSiN$_2$ and MgSiN$_2$ near the optical bandgap are presented in figure 5. It can be seen that these ternary nitrides are not direct band crystals. The valence band maximum (VBM) of MgSiN$_2$ occurs at the U(1/2, 0, 1/2) point while the conduction band minimum (CBM) lies at Γ. For comparison, the VBM of BeSiN$_2$ appears at Γ and the CBM occurs at X(1/2, 0, 0). From further comparison with the direct band result of GaN, the major cause for the indirect bandgap in these ternary nitrides could be attributed to the lower crystal symmetry of the orthorhombic structure.
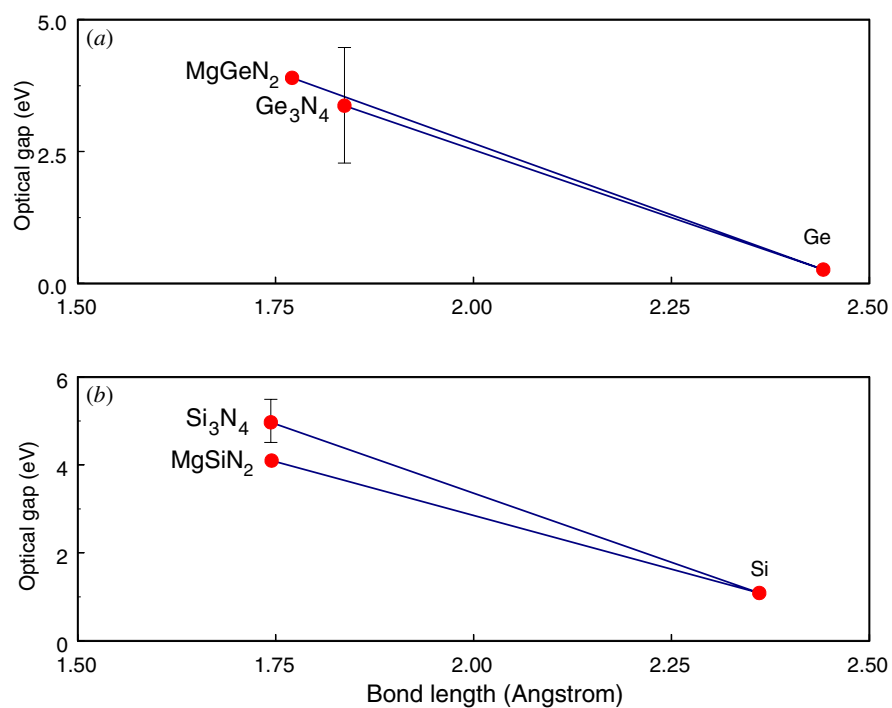
Figure 3. Comparison of the optical gap of orthorhombic ternary nitride crystal $MgXN_2$ ($Pna2_1$, X = Si, and Ge), with column IV and IV nitrides as a function of bond length.
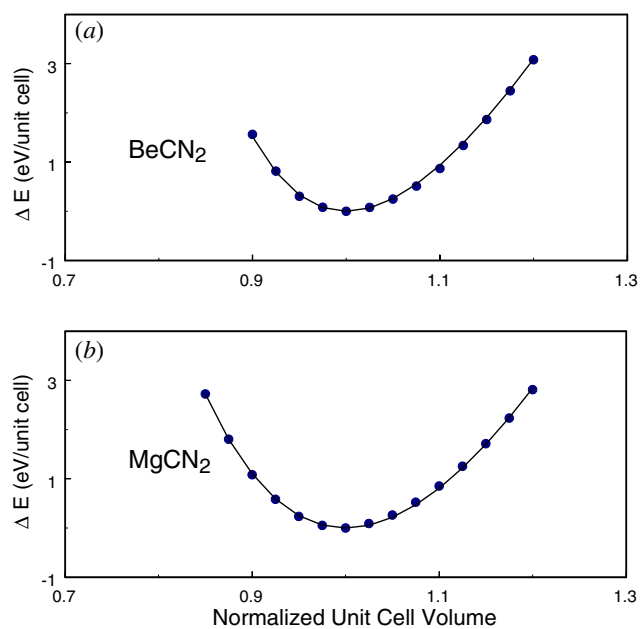

Figure 4. Calculated energy difference ($\Delta E = E(V) - E(V_0)$) as a function of normalized unit cell volume (V/V_0) for the ternary nitrides (a) $BeCN_2$ and (b) $MgCN_2$. The solid curves are the fits to equation (1).

Table 2. The calculated lattice constants (in Å) and mechanical properties of the orthorhombic ternary nitrides. Experimental data are given in parentheses whenever are available.

Nitride crystal ($Pna2_1$)	Unit cell dimensions (Å) ($\alpha = \beta = \gamma = 90°$)	B (GPa)	$B' = (\partial B/\partial P)_0$
BeCN$_2$	$a = 4.430$ $b = 5.301$ $c = 4.265$	374	6.2
MgCN$_2$	$a = 4.598$ $b = 6.219$ $c = 4.481$	234	3.7
BeSiN$_2$	$a = 4.942(4.98)^a$ $b = 5.748(5.75)^a$ $c = 4.651(4.67)^a$	270	12.7
MgSiN$_2$	$a = 5.267(5.28)^a$ $b = 6.483(6.46)^a$ $c = 5.011(4.98)^a$	175	1.0
BeGeN$_2$	$a = 4.986$ $b = 5.802$ $c = 4.694$	263	10.4
MgGeN$_2$	$a = 5.301(5.49)^a$ $b = 6.524(6.61)^a$ $c = 5.064(5.17)^a$	171	10.8
Ge$_3$N$_4$ ($P6_3/m$)^b	$a = 7.40$ $c = 3.20$	214	4.4

[a] Data taken from Inorganic Crystal Structure Database (ICSD), Fachinformationszentrum, Eggenstein-Leopoldshafen 2, D-7514 Karlsruhe, Germany.
[b] [14].

Table 3. Computed frequencies of zone-centre phonons (Γ), classified by symmetry label.

Nitride crystal ($Pna2_1$)	K (Group)	Irrep.	Frequencies (cm^{-1})
MgSiN$_2$	$\Gamma(C_{2v})$	A$_1$ ($z, x^2 + y^2, z^2$)	346, 354, 421, 544 614, 824, 836
		B$_1$ (x, xz)	465, 549, 706, 804
MgGeN$_2$	$\Gamma(C_{2v})$	A$_1$ ($z, x^2 + y^2, z^2$)	223, 324, 412, 524, 541, 738, 780
		B$_1$ (x, xz)	323, 487, 681, 768

To gain more insight into the calculated optical properties we studied PDOS and LDOS spectra. The calculated PDOSs for MgSiN$_2$ are given in figure 6. For the ternary nitride crystals studies here the valence bands are dominated by the bonding states of nitrogen. More specific features in the PDOS are presented as follows. The valence bands with bonding energy from -14.3 to -10.8 eV are mainly contributed from the N 2s states. The N 2p states dominate the electronic bands that are near the top of the valence bands ranging from -5.7 to 2.4 eV. The N bonding states are much higher than those of the electronic states of metal atoms (Mg and Si) in the absence of the metal d states. In contrast, all the antibonding states from nitrogen, and metal atoms, play significant roles in the conduction bands. Similar results were also found on group III nitride crystals XN (X: B, Al, Ga, In) [16].
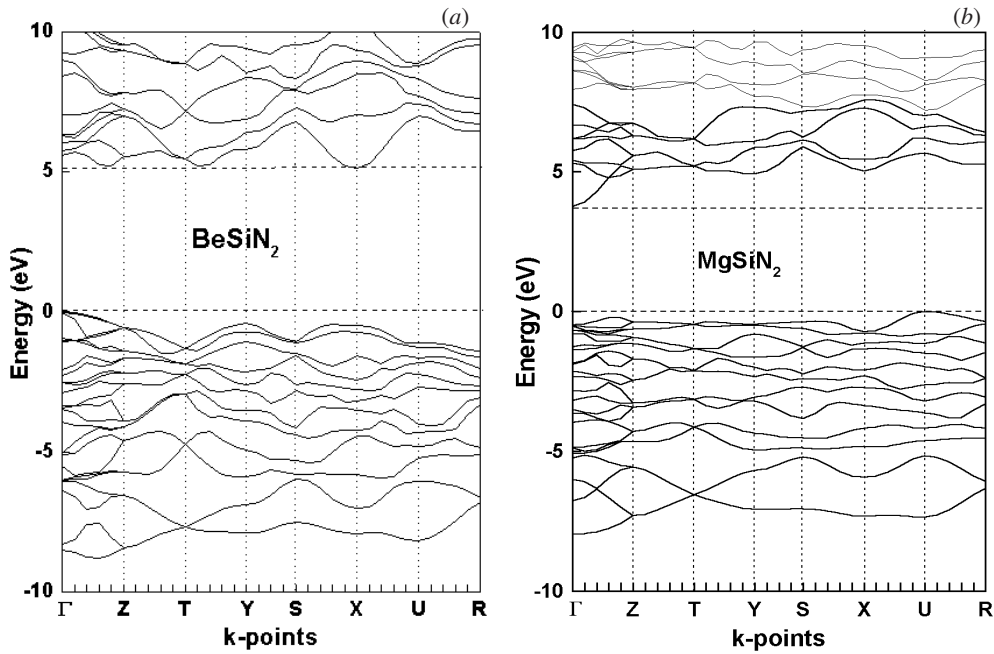
Figure 5. Electronic band structures of (*a*) BeSiN$_2$ and (*b*) MgSiN$_2$ near the optical gap.

3.3. Linear and second-order nonlinear optical susceptibilities

The calculated energy gap, dielectric constants, and second-order nonlinear susceptibilities are summarized in table 4. The anisotropy of static dielectric constants of these ternary nitrides is not significant. Although a small dissimilarity appears between the xx and yy components, the major birefringence lies between the zz and the xx components with a magnitude of about 0.1. Replacing Si with Ge increases the averaged dielectric constant from 4.61 to 4.79 accompanied with a decrease in the energy bandgap.

The frequency-dependent dielectric functions of MgSiN$_2$ are presented in figure 7. The first two peaks appearing at 4.5 and 5.0 eV in the imaginary part arise from the optical transitions from the VBM to CBM, which determine the absorption edge of MgSiN$_2$. From the PDOS analysis, we can find these transitions to have the characters of N 2p (at VBM) and the s orbitals of Mg, Si and N (at the CBM). Therefore the decreasing optical bandgap shown in table 4 can originate from a difference in the antibonding properties of metal atoms at the CBM.

Equation (6) has been used for analysing the static second-harmonic susceptibility of the ternary nitride crystals and the results are presented in table 4. For these materials, $\chi^{(2)}_{zzz}$ is negative with a fairly constant magnitude lying between -13.8 and -17.3 pm V^{-1}. In contrast all other susceptibility components such as $\chi^{(2)}_{xzx}$ and $\chi^{(2)}_{yzy}$ vary significantly with material. Note that bond additivity model predicts a simple relation of $\chi^{(2)}_{zzz} = -2\chi^{(2)}_{xxz}$ for wurtzite structure [17]. For ternary nitrides, we found that only MgGeN$_2$ follows this simple rule, while all other nitrides deviate considerably. For example, the ratio of $\chi^{(2)}_{xzx}$ and $\chi^{(2)}_{zzz}$ for MgSiN$_2$ is near to unity, but for BeSiN$_2$ the ratio can be as small as 0.1. Similar behaviour was also observed in group III nitrides [17], indicating that the simple bond additivity model is inappropriate for elucidating the nonlinear optical response in nitride crystals.
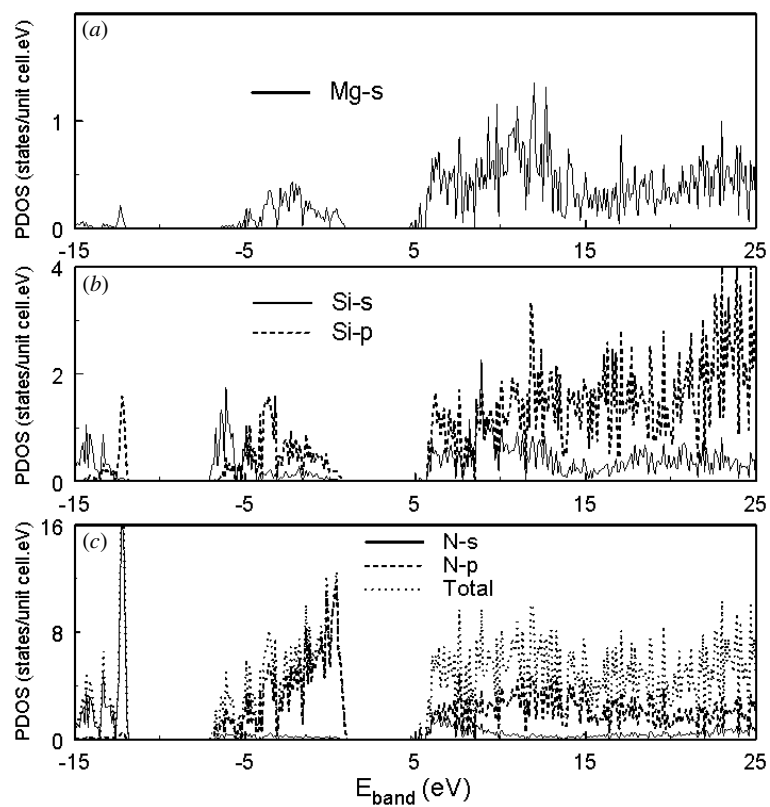
Figure 6. Partial densities of states of MgSiN$_2$ projected onto (*a*) Mg, (*b*) Si and (*c*) N species at various atomic orbitals.
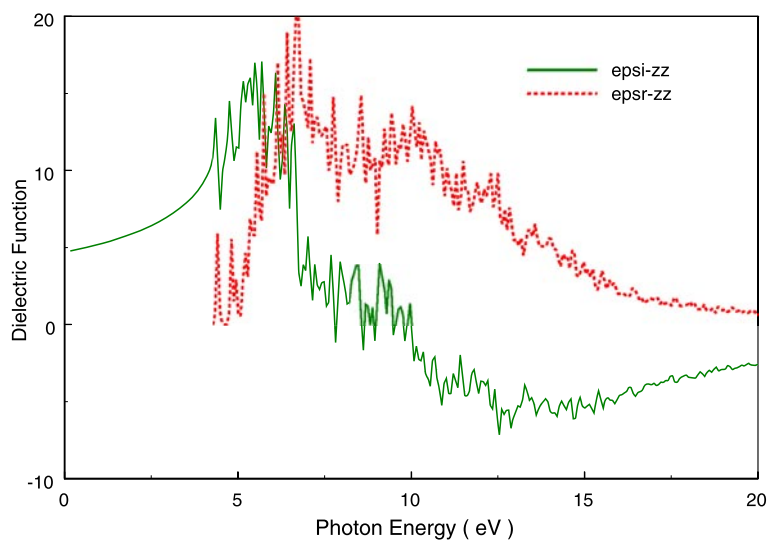

Figure 7. Real (solid curve) and imaginary (dashed) part of the optical dielectric function of MgSiN$_2$ as a function of incident photon energy.

Table 4. Calculated optical properties of the orthorhombic ternary nitrides.

Nitride crystal $(Pna2_1)$	Bandgap E_g (eV)	Dielectric constants	Second-order nonlinearity (pm V^{-1})
BeCN$_2$	5.75	$\varepsilon_{xx} = 4.74$	$\chi^{(2)}_{zzz} = -12.90$
		$\varepsilon_{yy} = 4.71$	$\chi^{(2)}_{xzx} = \chi^{(2)}_{zxx} = 4.73$
		$\varepsilon_{zz} = 4.89$	$\chi^{(2)}_{yzy} = \chi^{(2)}_{zyy} = 1.16$
MgCN$_2$	4.76	$\varepsilon_{xx} = 5.10$	$\chi^{(2)}_{zzz} = -13.81$
		$\varepsilon_{yy} = 5.00$	$\chi^{(2)}_{xzx} = \chi^{(2)}_{zxx} = 2.61$
		$\varepsilon_{zz} = 4.96$	$\chi^{(2)}_{yzy} = \chi^{(2)}_{zyy} = 13.38$
BeSiN$_2$	5.08	$\varepsilon_{xx} = 4.72$	$\chi^{(2)}_{zzz} = -17.09$
		$\varepsilon_{yy} = 4.77$	$\chi^{(2)}_{xzx} = \chi^{(2)}_{zxx} = 1.66$
		$\varepsilon_{zz} = 4.90$	$\chi^{(2)}_{yzy} = \chi^{(2)}_{zyy} = 1.12$
MgSiN$_2$	4.15	$\varepsilon_{xx} = 4.59$	$\chi^{(2)}_{zzz} = -17.30$
		$\varepsilon_{yy} = 4.57$	$\chi^{(2)}_{xzx} = \chi^{(2)}_{zxx} = 15.96$
		$\varepsilon_{zz} = 4.66$	$\chi^{(2)}_{yzy} = \chi^{(2)}_{zyy} = 14.82$
BeGeN$_2$	5.24	$\varepsilon_{xx} = 4.75$	$\chi^{(2)}_{zzz} = -18.14$
		$\varepsilon_{yy} = 4.72$	$\chi^{(2)}_{xzx} = \chi^{(2)}_{zxx} = 6.22$
		$\varepsilon_{zz} = 4.90$	$\chi^{(2)}_{yzy} = \chi^{(2)}_{zyy} = 3.47$
MgGeN$_2$	3.97	$\varepsilon_{xx} = 4.80$	$\chi^{(2)}_{zzz} = -14.49$
		$\varepsilon_{yy} = 4.71$	$\chi^{(2)}_{xzx} = \chi^{(2)}_{zxx} = 8.80$
		$\varepsilon_{zz} = 4.86$	$\chi^{(2)}_{yzy} = \chi^{(2)}_{zyy} = 7.58$

In such complex compounds as ternary nitrides, it is useful to identify the role played by each atomic species and orbital. For this purpose, we use equation (7) for resolving $\chi^{(2)}(0)$ into contributions from each atomic species at each energy interval in either the initial valence bands or intermediate conduction bands. The results are presented in figure 8 for BeSiN$_2$ and figure 9 for MgSiN$_2$. The main contributions to the SH susceptibilities of the orthorhombic ternary nitrides were found to originate from the electronic states near the optical bandgap. By comparing figure 8(*b*) with 9(*b*), we can also find that the various $\chi^{(2)}_{xzx}$ contributions from electronic bands of BeSiN$_2$ have more or less the same magnitude but with opposite signs. In contrast, for MgSiN$_2$ the positive terms dominate, which results in a larger $\chi^{(2)}_{xzx}$. Transition moments, which reflect the degree of inhomogeneity in the charge distribution of electronic bands, determine the sign of each term in equation (7). From the species and band-by-band decomposition, we found that all the atomic species contribute to the SH susceptibilities and there are no dominant species. Unlike borate crystals [18], the SH response in these ternary nitride crystals cannot be clearly separated into various terms from isolated atomic groups or clusters. This is expected from the ternary nitride structure whose metal atoms are tetrahedrally coordinated by N and vice versa both N atoms are tetrahedrally coordinated by the metal atoms $2 \times A$ and $2 \times B$. The full band method is therefore needed for correctly calculating the NLO response of these crystals.

Finally to reveal the reliability of our modelling, we applied the calculation method to wurtzite GaN. The choice of GaN is based upon its structural similarity to the ternary nitrides and the availability of numerous experimental and simulation results. The results are summarized in table 5. Our calculated unit cell dimensions are among the closest results to the experimental values. In addition, our bulk modulus agrees reasonably well with the measured values and also with other calculations. The calculated energy bandgap is about 30% smaller
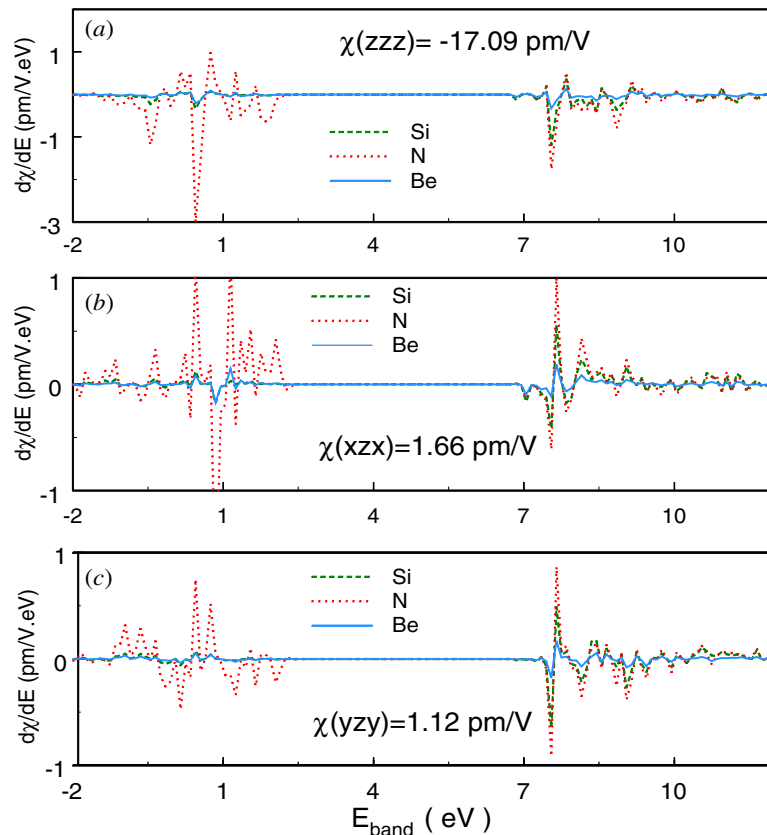
Figure 8. Second-order nonlinear optical susceptibility components (*a*) *zzz*, (*b*) *xzx* and (*c*) *yzy* of BeSiN$_2$ projected onto various atomic species and energy bands by using equation (7).

than the experimental observation; however, this is to be expected at the level of the LDA methodology. The smaller bandgap also overestimates optical dielectric constants. Although the smaller bandgap obtained with LDA can be corrected with a simple scissors approximation or more sophisticated GW correction, we did not intend to do so in this study. Our calculated second-order susceptibilities, which are about one half of the experimental values [8, 9], agree reasonably well with other calculated results with a similar theoretical sophistication [17]. Based on these comparisons, we can confidently conclude that the simulation results reported in this study reliably reflect the real physical properties of the ternary nitrides.

4. Conclusions

In summary, the structural, mechanical and optical properties of orthorhombic ternary nitride crystals have been analysed theoretically with a first-principles calculation scheme. These nitrides possess fairly large optical bandgap, second-order nonlinear optical susceptibility and bulk modulus. Therefore they could be useful for both optical and protective coating applications. Our calculations with band-by-band and atomic species decomposition not only yield values of material properties, but also provide deep insight into the fundamental understanding of the mechanical and optical properties of orthorhombic ternary nitrides.

Table 5. Lattice constants, elastic, and optical properties of wurtzite GaN.

|	$a = b$ (Å)	c s	B_0 (Gpa)	B'_0	E_g (eV)	$\varepsilon_\perp$	$\varepsilon_|$	ε_{av}	$\chi^{(2)}_{xzx}$ (pm V^{-1})	$\chi^{(2)}_{zzz}$ (pm V^{-1})
Present calculation	3.178	5.167	209	5.0	2.31	5.91	5.92	5.92	−9.0	15.9
Exp. [19]	3.190	5.200								
Exp. [20]	3.160	5.120								
Exp. [21]			188	3.2						
Exp. [22]			237	4.3						
Exp. [23]			245	4.0						
Exp. [24]					3.52					
Exp. [25]					3.30					
Exp. [26]								5.35		
Exp. [27]								5.80		
Exp. [28]									14.4	29.7
Exp. [29]									16.0	33.0
Other calc. [16]	3.240	5.240			2.40	5.87	5.89	5.88	−11.7	20.8
Other calc. [30]	3.170	5.130								
Other calc. [31]	3.162	5.142								
Other calc. [32]	3.143	5.111	215	5.9		5.21	5.41	5.28		
Other calc. [33]	3.220	5.260								
Other calc. [15]	3.143	5.111								
Other calc. [34]	3.146	5.125								
Other calc. [35]	3.170	5.135								
Other calc. [36]	3.162	5.141								
Other calc. [37]	3.126	5.120	190	2.9						
Other calc. [38]	3.210	5.237	197	—-						
Other calc. [39]			200	3.8		4.71	4.62	4.68		
Other calc. [40]					3.80					
Other calc. [17]						5.54	5.60	5.74	−6.9	11.5
Other calc. [41]									−4.2	7.0
Other calc. [42]									−8.5	12.1
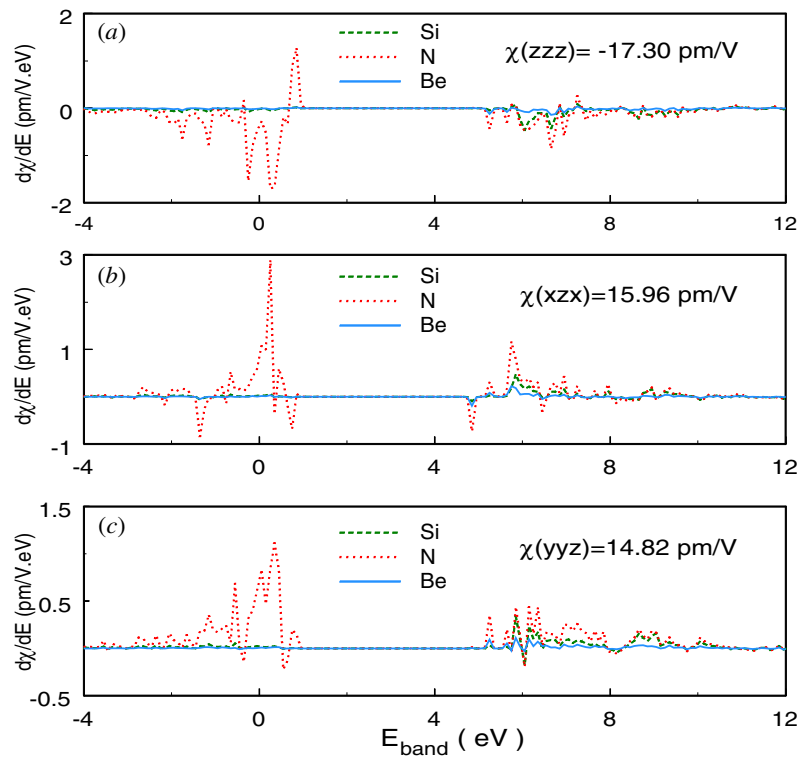
Figure 9. Second-order nonlinear optical susceptibility component (*a*) *zzz*, (*b*) *xzx* and (*c*) *yzy* of MgSiN$_2$ projected onto various atomic species and energy bands by using equation (7).

Acknowledgment

References

[1] Pankove J I and Moustakas T (ed) 1998 *Gallium Nitrides I (Semiconductor and Semimetals Vol 50)* (San Diego, CA: Academic)
[2] Chambouleyron I and Zanatta A R 2001 *J. Appl. Phys.* **84** 1
[3] Groen W A, Kraan M J and de With G 1993 *J. Eur. Ceram. Soc.* **12** 413
    Hintzen H T, Swaanen P, Metselaar R, Groen W A and Kraan M J 1994 *J. Mater. Sci. Lett.* **13** 1314
[4] Payne M C, Teter M P, Allan D C, Arias T A and Joannopoulos J D 1992 *Rev. Mod. Phys.* **64** 1045
[5] Monkhorst H J and Pack J D 1976 *Phys. Rev.* B **13** 5188
[6] Milman V, Lee M H and Payne M C 1994 *Phys. Rev.* B **49** 16 300
[7] Parlinski K, Li Z Q and Kawazoe Y 1997 *Phys. Rev. Lett.* **78** 4063
[8] Parlinski K 2001 *Phonon Software*
[9] Sanchez-Portal D, Artacho E and Soler J M 1996 *J. Phys.: Condens. Matter* **8** 3859
[10] Adolph B, Garrilenko V I, Tenelsen K, Bechstedt F and Del Sole R 1996 *Phys. Rev.* B **53** 9797
[11] Rashkeev S N, Lambrecht W R L and Segall B 1998 *Phys. Rev.* B **57** 3905
[12] Duan C G, Li J, Gu Z Q and Wang D S 1999 *Phys. Rev.* B **59** 369
[13] Bruls R J, Hintzen H T, Metselaar R and Loong C K 2000 *J. Phys. Chem. Solids* **61** 1285
[14] Lowther J E 2000 *Phys. Rev.* B **62** 5

[15] Karch K, Wagner J M and Bechstedt F 1998 *Phys. Rev.* B **57** 7043
[16] Gavrilenko V I and Wu R Q 2000 *Phys. Rev.* B **61** 2632
[17] Chen J, Levine Z H and Wilkins J 1995 *Appl. Phys. Lett.* **66** 1129
[18] Lin J, Lee M H, Liu Z P, Chen C and Pickard C J 1999 *Phys. Rev.* B **60** 13 380
[19] Schulz H and Thiemann K H 1977 *Solid State Commun.* **23** 815
     Maruska H P and Tietjen J J 1969 *Appl. Phys. Lett.* **15** 327
[20] Lagerstedt O and Monemar B 1979 *Phys. Rev.* B **19** 3064
[21] Xia H, Xia Q and Ruoff A L 1993 *Phys. Rev.* B **47** 12 925
[22] Ueno M, Yoshida M, Onodera A, Shimomura O and Takemura K 1994 *Phys. Rev.* B **49** 14
[23] Perlin P, Jauberthie-Carillon, Itie J P, San Miguel A, Grzegory I and Polian A 1992 *Phys. Rev.* B **45** 83
[24] Strite S, Rujian J, Li Z, Salvador A, Chen H, Smith D J, Choyke W J and Morkoc H 1991 *J. Vac. Sci. Technol.* B **9** 1924
[25] Landolt–Bornstein New Series 1982 *Numerical Data and Functional Relationships in Science and Technology,* Group III, vol 17 ed O Madelung, M Schulz and H Weiss (Berlin: Springer)
[26] Barker A S and Ilegems M 1973 *Phys. Rev.* B **7** 743
[27] Manchon D D, Barker A S, Dean P J and Zetterstrom R B 1970 *Solid State Commun.* **8** 1227
[28] Fujita T, Hasegawa T, Haraguchi M, Okamoto T, Fukui M and Nakamura S 2000 *Japan. J. Appl. Phys.* **39** 2610
[29] Zhang H Y, He X H, Shih Y H, Schurman M, Feng Z C and Stall R A 1996 *Appl. Phys. Lett.* **69** 2953
[30] Kim K, Lambrecht W R L and Segall B 1996 *Phys. Rev.* B **53** 16 310
[31] Wright A F and Nelson J S 1994 *Phys. Rev.* B **50** 2159
     Wright A F and Nelson J S 1995 *Phys. Rev.* B **51** 7866
[32] Karch K and Bechstedt F 1997 *Phys. Rev.* B **56** 7404
     Karch K and Bechstedt F 1998 *Phys. Rev.* B **57** 7043
[33] Vogel D, Kruger P and Ho K M 1992 *Phys. Rev.* B **45** 1159
[34] Miwa K and Fukumoto A 1993 *Phys. Rev.* B **48** 7897
[35] Kim K, Lambrecht W R and Segall B 1996 *Phys. Rev.* B **53** 16 310
[36] Wright A F and Nelson J S 1994 *Phys. Rev.* B **50** 2159
[37] Van Camp P E, Van Doren V E and Derreese J T 1992 *Solid State Commun.* **81** 23
[38] Shimada K, Sota T and Suzuki K 1998 *J. Appl. Phys.* **84** 4951
[39] Christensen N E and Gorezyca I 1994 *Phys. Rev.* B **50** 4397
[40] Vogel D, Kruger P and Pollmann J 1997 *Phys. Rev.* B **55** 12 836
[41] Chen J, Jonsson L, Wilkins J W and Levine Z H 1997 *Phys. Rev.* B **56** 1787
[42] Hughes J L P, Wang Y and Sipe J E 1997 *Phys. Rev.* B **55** 13 630